Available online at www.sciencedirect.com
ScienceDirect
Journal of Magnetic Resonance 190 (2008) 271–279
JMR Journal of Magnetic Resonance
www.elsevier.com/locate/jmr

Design of phase-modulated broadband refocusing pulses

Rolf F. Schulte [a,*], Patrick Le Roux [b], Mika W. Vogel [a], Hartmut Koenig [a]

[a] GE Global Research, Munich, Germany
[b] GE Healthcare, Applied Science Lab, Buc, France

Received 30 March 2007; revised 23 July 2007
Available online 13 November 2007

Abstract

Broadband linear-phase refocusing pulses were designed with the Shinnar–Le Roux (SLR) transformation and verified experimentally. The design works in several steps: initially, a linear-phase B polynomial is created with the Parks–McClellan/Remez exchange algorithm. The complementary A polynomial required for the SLR transformation is generated with the Hilbert transformation, yielding the minimum-phase response. The phase response of the A polynomial is altered by zero-flipping, which changes the overall pulse shape while retaining its refocusing profile. Optimal pulses in terms of minimal $B_{1\max}$ and hence broadest bandwidth were found with non-linear optimisation of the zero-flipping pattern. These pulses are generally phase modulated with a time-symmetric amplitude and anti-symmetric phase modulation. In this work, a whole range of pulses were designed to demonstrate the underlying relationships. Five exemplary pulses were implemented into a PRESS sequence and validated by acquiring images of a water–oil phantom and lactate spectra at TE = 144 ms.

Keywords: Radio-frequency pulse design; Shinnar–Le Roux (SLR) transformation; Phase-modulation; Broadband refocusing pulses

1. Introduction

Spin–echo experiments require radio-frequency (RF) pulses, which refocus the magnetisation of interest. In the field of *in-vivo* MRI and MRS, these pulses are shaped to yield a desired refocusing profile and become spatially selective by superposition of linear gradients on the magnetic field. The bandwidths of these refocusing pulses are strictly limited by the maximum RF field strength ($B_{1\max}$) of the MR scanner and coil. This limitation in bandwidth leads to a relative spatial displacement of species with different chemical shifts, known for instance as water–fat shift in MRI or chemical-shift-displacement artefact in MRS.

The chemical-shift displacement is aggravated at higher field strengths, since the chemical shift is proportional to B_0, whereas $B_{1\max}$ and hence bandwidth of RF pulses generally decreases due to hardware and power deposition constraints. On whole-body MR scanners with $B_0 = 3$ T, the relative displacement of water and fat is in the range of 50% of the slice thickness. Therefore, PRESS [1], a popular MRS localisation technique, is heavily impaired and generally does not yield satisfactory results for $B_0 \geqslant 3$ T. PRESS is a double spin-echo experiment with one slice-selective excitation pulse and two slice-selective refocusing pulses, all spatially selective in orthogonal directions. Therefore, the resulting spin echo stems from a localised single voxel in three-dimensional space. Especially problematic for PRESS at higher field strengths is anomalous J modulation, which leads to an almost complete signal cancellation for lactate at TE = 144 ms [2–4]. Anomalous J modulation denotes the effect of a spatially varying J evolution due to displacements of the coupling partners. The PRESS box exhibits eight regions of different J evolutions, one where the coupling partner experiences all three pulses, six regions where it experiences only selected pulses and one where it does not experience any pulse at all. The final spectrum is the superposition of these different evolutions.

Various alternatives to PRESS are applied for volume localisation in MRS at higher field strengths, such as

* Corresponding author.
E-mail address: rolf.schulte@research.ge.com (R.F. Schulte).

1090-7807/$ - see front matter © 2007 Elsevier Inc. All rights reserved.
doi:10.1016/j.jmr.2007.11.008

STEAM [5] or LASER [6,7]. STEAM works with three 90° pulses, which naturally have much broader bandwidths than refocusing pulses. However, STEAM suffers from a signal loss of about 50%. LASER, a localisation sequence with three pairs of adiabatic full passage pulses, is better in terms of signal yield. Pairs of pulses with the same slice-selection gradients are used in order to compensate the non-linear phase induced by a single adiabatic pulse. The resulting sequence is robust, however at the cost of a fairly long minimum echo time due to the long duration of six refocusing pulses.

Another approach to improve MRS localisation is over-prescribed PRESS [8,9], where normal PRESS localisation is combined with outer-volume suppression. The PRESS box is enlarged and the region of chemical-shift displacement is saturated with quadratic-phase RF pulses before the experiment [8,10,11]. This considerably increases energy deposition and deteriorates water suppression, which is also preceding the PRESS experiment. A promising alternative to STEAM, LASER and over-prescribed PRESS is to use broadband linear-phase refocusing pulses [12–15] in the PRESS sequence. However, this class of pulses and their design is rather unknown.

RF pulse design is a difficult task and many methods have been proposed over the years. The spin evolution in MRI can be described with the coupled differential Bloch equations, which cannot be inverted analytically in most cases. For small flip angles, it is possible to approximate the Bloch equations by the Fourier transformation assuming $\dot{M}_z = 0$, which holds for angles up to approximately 40°–50°. The error in the desired target profile is intolerable for refocusing pulses due to the large flip angle of 180°.

An elegant and versatile approach for RF pulse design is the Shinnar-Le Roux (SLR) transformation [16], which reversibly transforms an RF pulse into two finite-impulse-response (FIR) filters, namely the "A" and "B" polynomials. The problem of RF pulse design is thus reduced to FIR filter design, which is a highly-developed engineering task with many different methods existing. The most common class of RF pulses have a linear phase. For refocusing pulses this traditionally leads to time-symmetric pulses with only real coefficients (i.e., no phase modulation). The second half of the pulse refocuses the phase acquired during its first half, and hence no undesired phase remains. It is also possible to design pulses with a non-linear phase response, such as minimum, maximum [16], quadratic [10,11] or higher-order polynomial [17]. The phase can also be altered by zero-flipping [18–20], which has the interesting feature of changing only the phase while retaining its magnitude response. However, non-linear phases remain in the refocusing profiles and cannot be compensated by (fast-switching) linear gradients present on common MRI scanners. Non-linear phase pulses can be applied twice, hence the second pulse compensates the non-linear phase acquired by the first one [21], which is the principle of LASER [6,7].

A different approach for increasing the bandwidth of refocusing pulses is to deviate from the traditional sinc-Gaussian type of pulse shapes. In general, refocusing pulses must have a time-symmetric magnitude and anti-symmetric phase modulation ([13] and Appendix A). This kind of pulses can be designed by direct solution of the Bloch equations with non-linear optimisation [13], concatenation of self-refocused 90° excitation pulses [22], or the SLR transformation in combination with zero-flipping of A [12,14,15]. For the SLR approach, a standard linear-phase B polynomial is designed and combined with a non-minimum-phase A polynomial. A few single pulses appeared mainly in conference proceedings. However, no systematic investigation and verification was reported for this class of pulses.

The objectives of this work are to extend the design principles of broadband refocusing pulses, investigate the underlying relationships and verify several exemplary pulses experimentally. For the design of broadband refocusing pulses, a standard linear-phase B polynomial was designed with the Remez exchange algorithm [23]. The corresponding minimum-phase A polynomial was created with the Hilbert transformation and then altered in its phase response by zero-flipping [18–20]. There are 2^p different combinations of flipping the zeroes and hence as many different phase functions existing (with p denoting the zeroes in the passband). Finding the optimal combination of zeroes to flip for the minimal $B_{1\max}$ is an intricate optimisation problem, particularly for pulses with high-time bandwidth products. Therefore, two different optimisation strategies for flipping the ideal combinations of zeroes are proposed: an exhaustive search, where all combinations are considered and a genetic algorithm. Several favourable pulses are selected, implemented into the PRESS sequence [1] and verified experimentally by measuring their refocusing profile in a water–oil phantom and a lactate spectrum at an echo time of 144 ms.

2. Theory

The SLR transformation reversibly transforms an RF pulse into two FIR filters, the "A" and "B" polynomials

$$\begin{aligned} A(z) &= \sum_{j=0}^{n-1} a_j z^{-j}, \\ B(z) &= \sum_{j=0}^{n-1} b_j z^{-j}, \end{aligned} \tag{1}$$

with $z = \mathrm{e}^{\mathrm{i}\omega}$ and the normalised angular frequency $-\pi \leqslant \omega \leqslant \pi$. Evaluation along the unit circle yields the frequency responses $A(\omega)$ and $B(\omega)$, which is equivalent to the Fourier transformation. The SLR transformation requires

$$|A(\omega)|^2 + |B(\omega)|^2 = 1. \tag{2}$$

The task in the SLR pulse design is to find appropriate A and B FIR filters. In the case of refocusing pulses, the profile for spin-echoes with surrounding crusher gradients is given by [16]

$$M_{xy}^{+}(\omega) = -z^{n}B^{2}(\omega)M_{xy}^{-*}(\omega), \tag{3}$$

where M_{xy}^{+} and M_{xy}^{-} denote the transverse magnetisation after and before the pulse, respectively. That is, the A polynomial has no influence on the refocusing profile, but is constrained in its magnitude response by

$$|A(\omega)| = \sqrt{1 - |B(\omega)|^{2}}, \tag{4}$$

in order to fulfil Eq. (2). The phase is unconstrained and can be freely chosen as long as it can be represented by a polynomial in z. Using different A polynomials can considerably alter the resulting RF pulse shape. That means, many different RF pulse shapes can describe exactly the same refocusing profile given by $B^{2}(\omega)$ (Eq. (3)), including its phase response and error ripples.

Obtaining an appropriate phase to the magnitude response $|A(\omega)|$ is called phase retrieval and amounts to an inverse problem. One simple and special solution is the minimum-phase polynomial, which is an analytic signal [24]. The log-magnitude and phase response are Hilbert transform pairs. Hence, the minimum-phase for $|A(\omega)|$ can be calculated with the Hilbert transformation ($\mathscr{H}$) [16]

$$\angle A(\omega) = \mathscr{H}\{\log|A(\omega)|\}. \tag{5}$$

The minimum-phase A polynomial is advantageous in the sense that it yields RF pulses with the minimal energy deposition [16]. An A polynomial with a different phase function, however, can decrease the peak B_1 value of the RF pulse ($B_{1\max}$). This allows to shorten the pulse and hence increase its bandwidth.

Solutions with non-minimum phases are more difficult to obtain. One way to approach this inverse problem is zero-flipping [18–20]. The complex A polynomial is factored out into its zeroes ρ_k according to

$$A(z) = \sum_{j=0}^{n-1} a_j z^{-j} = c \cdot \prod_{k=1}^{n-1}(1 - z^{-1}\rho_k), \tag{6}$$

where c is a scaling constant. All zeroes are located inside the unit circle (i.e., $|\rho_k| < 1$), because A is a minimum-phase polynomial. Mirroring a zero on the unit circle to one over its radius alters the phase but not the magnitude response. Formally, this zero-flipping is given by replacing a zero with one over its complex conjugate

$$\rho_k' = \frac{1}{\rho_k^{*}}. \tag{7}$$

This process can be performed for multiple zeroes. The altered A polynomial can then be calculated again by replacing the respective zeroes in Eq. (6) and a subsequent scaling (i.e., determination of c) for instance with Eq. (2). The drawback of flipping zeroes of the A polynomial is an increase in energy deposition. The difference in energy deposition from the minimum-energy solution ΔE expressed in units of tesla^2, is given by [25,26]

$$\Delta E = -\frac{8n}{\gamma^{2}\tilde{T}} \sum_{l} \log|\rho_l|, \tag{8}$$

where n is the filter length, $\tilde{T}$ the total pulse duration and l the index of the flipped zeroes.

The objectives in the design of broadband refocusing pulses are to find the optimal combinations of flipped zeroes yielding RF pulses with the minimal $B_{1\max}$. The amount of different combinations is given by 2^{p}, where p denotes the number of considered zeroes. One great simplification stems from the fact that only zeroes flipped in the passband of the pulse (i.e., $-BW/2 \leqslant \omega \leqslant BW/2$) beneficially change the pulse shape. The number of zeroes in this passband is related to the time-bandwidth product by

$$p \approx \frac{n \cdot \mathrm{BW}}{2\pi}. \tag{9}$$

The total filter length n has no influence on the number of zeroes in the passband.

3. Methods

Broadband refocusing pulses are designed with the following steps. First, a linear-phase B polynomial is designed with the Parks–McClellan/Remez-exchange algorithm [23]. Then, the corresponding minimum-phase A polynomial is generated with the Hilbert transformation (Eq. (5)). The A polynomial is factored out into its zeroes and some are flipped (Eq. (7)). The zeroes are multiplied to yield the new non-minimum phase A polynomial (Eq. (6)), which is scaled with Eq. (2). Both the A and B polynomials are finally transformed into an RF pulse with the inverse SLR transformation [16]. The only question remaining is which zeroes need to be flipped in order to find the pulse with the minimum $B_{1\max}$.

Two different non-linear optimisation techniques were applied to determine the zero-flipping pattern: an exhaustive search and a genetic algorithm [27]. The exhaustive search has the advantage of always finding the global minimum. However, the computational expense quickly aggravates, hence permitting only a small number of zeroes to be systematically combined. In the current work, the number of zeroes to be combined was limited to 13.

The second optimisation approach was a genetic algorithm [27]. The initial populations are given in two different ways, random or systematic. For good results, the random initialisation has to be fairly large, thus we chose an initial population size of $6 \cdot 1.3^{p}$, where p denotes the number of zeroes in the passband. The other kind of initial population included no zeroes, a single zero and a combination of two different zeroes flipped.

The B polynomials designed with the Parks–McClellan/Remez-exchange algorithm have an equi-ripple error response. The most equitable comparison of pulses with

different time-bandwidth products can be made by designing FIR filters with the same error ripple, which is a function of the empirically derived performance measure D_∞ [16]. This D_∞ is related to the filter length n, (angular) bandwidth BW and fractional-transition width FTW by

$$D_\infty = n \cdot \mathrm{BW} \cdot \mathrm{FTW}. \tag{10}$$

Note, that D_∞ as well as BW are given in this work in units of radian, consistent to [11,17] but in contrast to [16] with an additional factor of 2π.

A whole range of pulses were designed with an effective flip angle of $\theta = 168°$ to gain additional insight into the pulse design. The SLR transformation has a singularity at 180° (Eq. (2)). In order not to exceed this limit with the large error ripples for $D_\infty = 10$ in the pass band, we had to reduce θ to 168°. The pass band was weighted 100 times as much as the stop band. Four series of comparable pulses (i.e., same error ripples) were designed with $D_\infty = 10, 15, 20$ and 25, respectively. The time-bandwidth products were $n \cdot \mathrm{BW} = 25, 30, 35, \ldots, 500$ (in radian), which results in fractional-transition widths according to Eq. (10) of 0.02 to 1. For comparison, traditional sinc-Gaussian type of pulses were designed for all series with the same B polynomials and the minimum-phase A polynomials.

In a second series, D_∞ was fixed to a constant value of 20, leading to reasonable pass band ripples. This permitted a nutation angle of $\theta = 172°$ even with equal weight on pass and stop bands. The time-bandwidth product was again varied in the same range of $n \cdot \mathrm{BW} = 25$ to 500 and also in steps of 5. From that series, five exemplary pulses were selected and implemented into the standard PRESS sequence. Their profile was measured with an imaging sequence (TR = 1 s and 160×256 phase and frequency encodes, respectively). The effect of broadband refocusing pulses on the J evolution of lactate was shown by measuring a phantom containing 100 mM lactate, 3 mM TMS, 100 mM sodium formate and 10 mM sodium azide (PRESS with TE = 144 ms, TR = 2 s and 64 averages).

All experiments were performed on GE 3T HD Signa 12M4 scanner (GE Healthcare, Milwaukee, WI, USA) equipped with a transmit-receive head coil. A water–oil phantom was prepared with sunflower oil and water doped with 0.5 mM DOTAREM (Guerbet, Roissy, France). All routines were implemented in Matlab V7.1 (R14) SP3 (The MathWorks, Natick, MA, USA). The genetic algorithm from the "Genetic Algorithm and Direct Search Toolbox" was used.

4. Results and discussion

It is possible to design a wide range of useful RF pulses with the proposed optimisation methods (Figs. 1 and 2). Beyond certain time-bandwidth products, i.e., zeroes in the passband (Eq. (9)), the optimisations become impractical (>1 day on a current PC). The exhaustive search is feasible up to $n \cdot \mathrm{BW} \approx 125$ (red line in Fig. 1), while the genetic algorithm with a large random initial population extends up to $n \cdot \mathrm{BW} \approx 225$ (cyan line in Fig. 1). The genetic algorithm with a systematic initial population is computationally feasible up to $n \cdot \mathrm{BW} = 500$ and beyond (green line in Fig. 1). The genetic algorithm does not always find the global minimum, especially with the relatively small systematic initial populations. This effect can be observed in Fig. 1, where pulses obtained with the exhaustive search, hence the global optimum, sometimes exhibit larger bandwidths for the same time-bandwidth product as the pulses optimised with the genetic algorithm.

Broadband and traditional pulses are scaled to a maximum RF field strength of $B_{1\,\mathrm{max}} = 24$ μT and plotted over the pulse durations (Figs. 1 and 2). The most important observation is that the broadband refocusing pulses allow for an approximately linear increase of bandwidth with pulse duration. This is in contrast to the fixed bandwidth

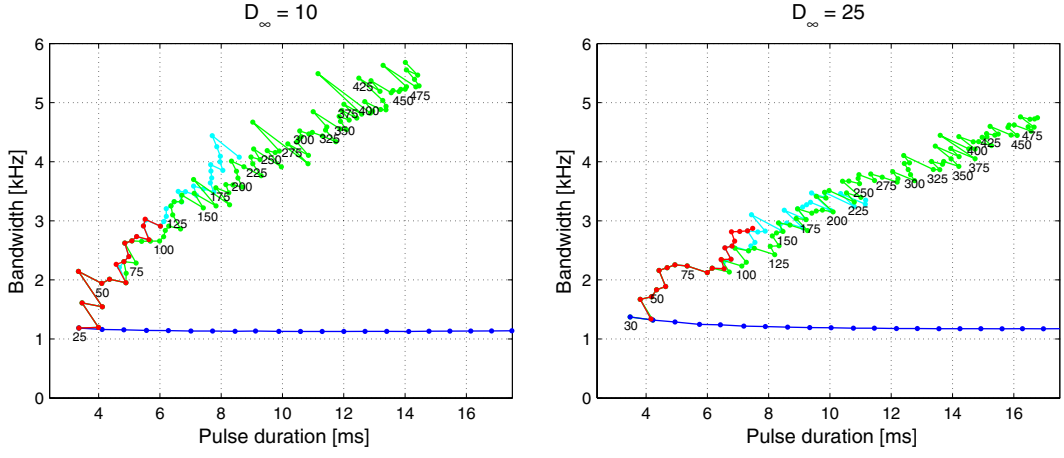

Fig. 1. The resulting physical bandwidths and pulse durations, when scaling the pulses to $B_{1\mathrm{max}} = 24$ μT for different error ripples ($D_\infty = 10$ and 25) and time-bandwidth products from 25 (left) to 500 (right) in steps of 5. The broadband refocusing pulses were optimised by exhaustive search (red) and the genetic algorithm with random (cyan) and systematic (green) initial populations. For comparison, traditional pulses are shown in blue. (For interpretation of the references to colour in this figure legend, the reader is referred to the web version of this paper.)

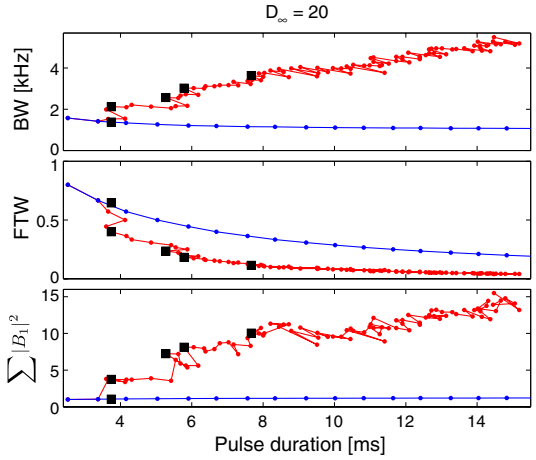

Fig. 2. RF pulses with $\theta = 172^\circ$ and $D_\infty = 20$. This time only pulses with the smallest $B_{1\max}$ of the three optimisation methods were selected. The bandwidth (upper row) is plotted along with the fractional-transition width (FTW) (middle) and relative energy $\sum |B_1|^2$, normalised to the pulse with $n \cdot \mathrm{BW} = 25$ (bottom). The five selected exemplary pulses are depicted by black rectangles.

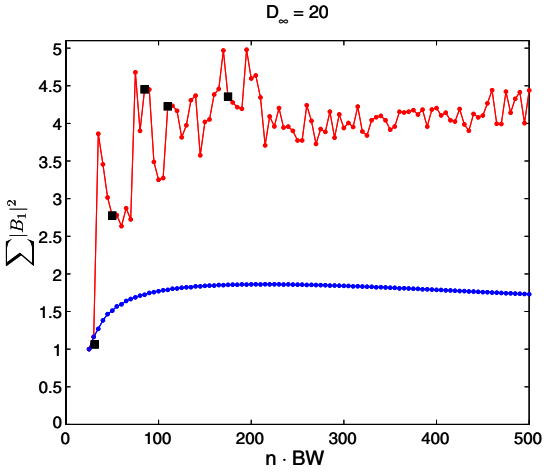

Fig. 3. Energy plotted over the time-bandwidth products for pulses scaled to the same physical bandwidth. This shows the additional increase in energy deposition due to zero flipping, excluding the effect of different bandwidths.

of traditional sinc-Gaussian type of pulses (blue line in Figs. 1 and 2),[1] where the number of side-lobes is mainly influencing the selectivity but not the bandwidth.

Along with broader bandwidth comes also better selectivity and higher energy deposition (Fig. 2). Traditional pulses improve their selectivity with one over the pulse duration, while broadband pulses improve much faster. However, the disadvantage is a higher energy deposition by broadband pulses (Fig. 2, bottom row), both inherently (Eq. (8) and Fig. 3) and because the energy is proportional to the bandwidth. All pulses are scaled to the same physical bandwidth in Fig. 3 in order to elucidate the additional energy deposited by broadband refocusing pulses. It is interesting to note in this figure that the optimal pulses in terms of broadest bandwidth do not necessarily induce the highest energies.

One traditional and four broadband refocusing pulses were selected from the series in Fig. 2 for a further comparison and validation. The physical parameters of the pulses when scaling them to $B_{1\max} = 24$ μT are listed in Table 1. These parameters include pulse duration, bandwidth, fractional transition width and the energy deposition (SAR). Along with broader bandwidth comes a longer pulse duration and more SAR. In MR experiments both duration and SAR is limited, hence we chose pulses only in a practically useful range ($n \cdot \mathrm{BW} \leqslant 175$). The RF pulse shapes are plotted in Fig. 4 (left column). As predicted by theory [13], the amplitude modulation of broadband refocusing pulses is time symmetric, whereas the phase modulation is time anti-symmetric. This is also derived in Appendix A in the context of the SLR transformation. There are no direct constraints to this symmetry during the design process,

Table 1
Parameters for the five exemplary pulses ($n \cdot \mathrm{BW} = 31$ is traditional, rest broadband)

$n \cdot$ BW (rad)	$\tilde{t}$ (ms)	$\widetilde{\mathrm{BW}}$ (kHz)	FTW	E (same $B_{1\max}$)	E (same $\widetilde{\mathrm{BW}}$)
31	3.7	1.4	0.65	1.06	1.06
50	3.7	2.1	0.4	3.75	2.78
85	5.3	2.6	0.24	7.24	4.45
110	5.8	3.0	0.18	8.12	4.23
175	7.7	3.6	0.11	10.05	4.36

The physical parameters pulse duration $\tilde{t}$ and bandwidth $\widetilde{\mathrm{BW}}$ are for $B_{1\max} = 24$ μT. The energies are normalised to a traditional sinc-Gaussian type of RF pulse with $n \cdot \mathrm{BW} = 25$.

hence it is solely a result of modifying the phase response of A. Only zero flipping the A polynomial can alter the RF pulse shape without affecting the refocusing profile. It becomes clear from Eq. (3), that zero flipping the B polynomial will alter both pulse shape and phase response of the refocusing profile.

The sensitivity to wrong scaling of the RF amplitude is shown in the middle column of Fig. 4. This comparison is important because B_1 homogeneity is often impaired at higher field strengths ($B_0 \geqslant 3$T) and in larger objects (e.g., human body). Units on the y-axis are given in percent, with 100% corresponding to correct B_1 amplitude scaling. The physical bandwidth in hertz is plotted along the x-axis, while the refocusing profile (M_x) is represented by the contours in colour[2] code. Cross-sections through $B_1 = 100\%$ (Fig. 5, left) show the improvements in bandwidth and selectivity. The traditional pulse ($n \cdot \mathrm{BW} = 31$) is fairly robust to wrong RF scaling, as can be seen by the long plateau with $M_x > 0.9$ in Fig. 4. The sensitivity

[1] For interpretation of the references to colour in Fig. 2, the reader is referred to the web version of this paper.

[2] For interpretation of the references to colour in this figure, the reader is referred to the web version of this paper.

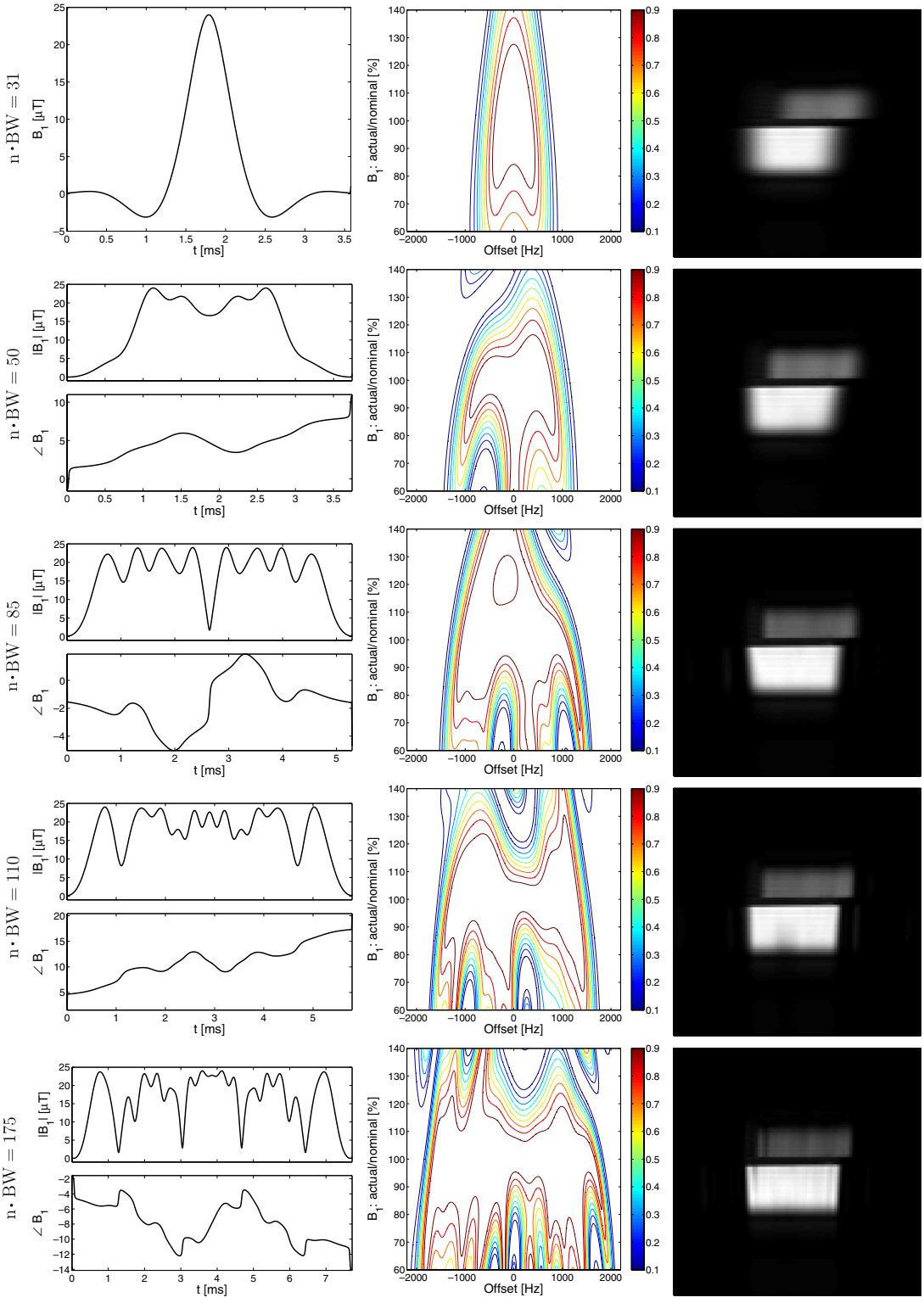

Fig. 4. The five exemplary pulses (left), their refocusing profiles in dependence of B_1 deviations (middle), and the experimental verification in a water–oil phantom (right).

of broadband refocusing pulses to B_1 inhomogeneities is increasing with the time-bandwidth product, leading to a fairly complex band pattern (e.g., $n \cdot \mathrm{BW} = 175$ with $B_1 = 70\%$).

Fig. 4 (right column) shows the experimental verification of the five exemplary pulses in the water–oil phantom. The spin-echo sequence is composed of a PRESS volume localisation with the excitation and refocusing being in vertical and horizontal direction, respectively. The minimum echo time was chosen ($\mathrm{TE} = 26, 26, 30, 31, 34$ ms for $n \cdot \mathrm{BW} = 31, 50, 85, 110, 175$, respectively), which increased due to longer pulse durations. The gradient strengths were

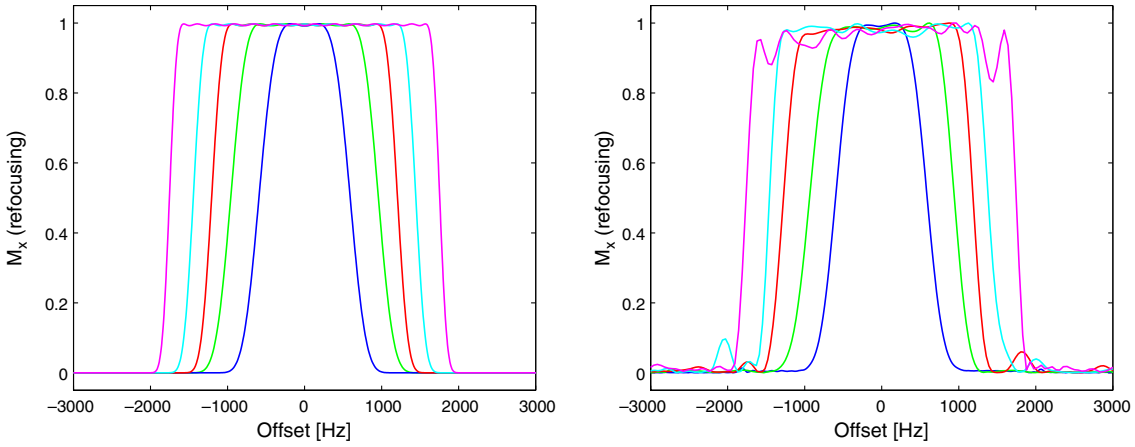

Fig. 5. Transverse magnetisation (M_x) for the five exemplary pulses ($n \cdot \mathrm{BW} = 31$; 50; 85; 110; 175 from inside out). The left and right plot show the ideal refocusing and the cross-sections through the measured profiles from Fig. 4, respectively.

adapted to always select the same voxel size. The chemical-shift displacement artefact is considerably reduced when using broader bandwidths, while the selectivity is improved. Cross-sections through the water part of the images are shown in Fig. 5 on the right. These refocusing profiles degrade slightly for the broadest bandwidths. As discussed in the last paragraph, this is due to an increased sensitivity to B_1 inhomogeneity.

The last validation of the exemplary pulses is through spectroscopic measurement of lactate with a PRESS sequence at TE = 144 ms. Ideally, lactate shows up as an inverted doublet (TE = $1/J$). This is almost achieved with $n \cdot \mathrm{BW} = 175$, as visible in Fig. 6. The J evolution of lactate is heavily impaired for PRESS localisation with narrow-bandwidth pulses (anomalous J modulation). This can be observed in Fig. 6 for the traditional refocusing pulse ($n \cdot \mathrm{BW} = 31$), where the signal is reduced and the doublet almost in anti-phase. The signal cancellation will be even more severe for shims *in vivo* of $\geqslant 7$ Hz, instead of the phantom shim of ≈ 2 Hz.

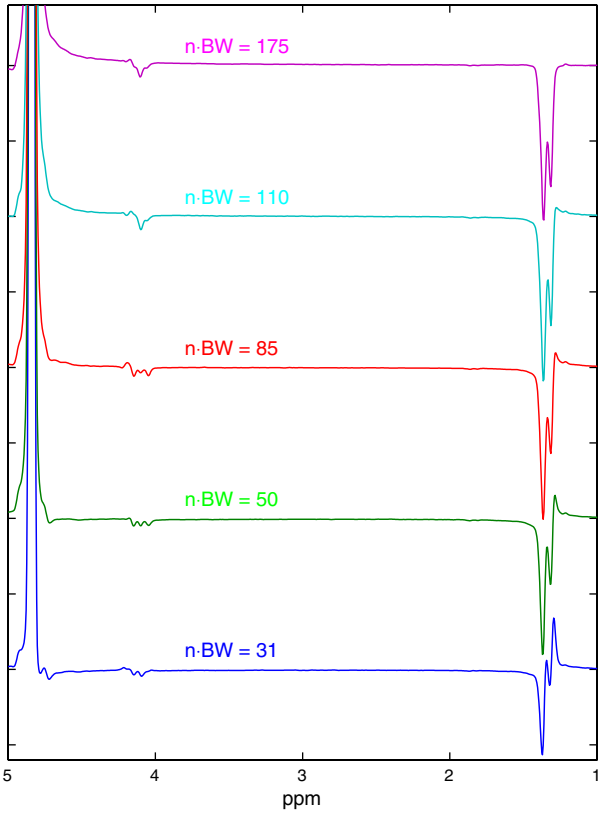

Fig. 6. Lactate evolution for PRESS localisation with TE = 144 ms. Insufficient bandwidth of the refocusing pulse leads to anomalous J evolution (spectrum at the bottom), which can be considerably reduced with broadband refocusing pulses (top).

5. Conclusions

The design of broadband refocusing pulses presented in this work is flexible, provides a good understanding of the nature of the problem and yields practical pulses. The broadband refocusing pulses enable a considerable increase in bandwidth along with much better selectivity. The drawbacks are a higher energy deposition and a higher sensitivity towards wrong scaling of the RF amplitude. One possibility to decrease this sensitivity could be to apply non-linear optimisation [13], and use the presented broadband refocusing pulses for initialisation.

PRESS localisation greatly benefits from broadband refocusing pulses. The chemical-shift-displacement artefact is alleviated, which will be even more important for spectroscopy at 7 T. Using PRESS with broadband refocusing pulses is a viable alternative to other localisation methods applied on high-field scanners, such as STEAM and LASER. Furthermore, the problem of anomalous J modulation can be greatly reduced.

Acknowledgments

This work was co-funded by the Bavarian state ministry (StMWIVT), chapter 0703, title 68668.

The exemplary pulses are available on request.

Appendix A

In this appendix, we demonstrate in the context of the SLR algorithm that refocusing pulses must have a time symmetric amplitude and anti-symmetric phase modulation. The derivations are similar to Murdoch's findings [13], however we use spinors (SU_2 matrices) instead of 3×3 (SO_3) rotation matrices. The SLR algorithm [16] represents a train of n-hard-pulses in the form of a product of SU_2 matrices with interleaved nutations (C_j, S_j) and precessions $(z = e^{i\omega})$

$$\begin{bmatrix} \alpha_n & -\beta_n^* \\ \beta_n & \alpha_n^* \end{bmatrix} = \begin{bmatrix} C_n & -S_n^* \\ S_n & C_n \end{bmatrix} \cdots \begin{bmatrix} C_2 & -S_2^* \\ S_2 & C_2 \end{bmatrix} \begin{bmatrix} z^{1/2} & 0 \\ 0 & z^{-1/2} \end{bmatrix} \cdot \begin{bmatrix} C_1 & -S_1^* \\ S_1 & C_1 \end{bmatrix}. \tag{11}$$

The nutations $C_j = \cos(\phi_j/2)$ and $S_j = e^{i\theta_j}\sin(\phi_j/2)$ are composed of a rotation about the RF field ϕ_j and an RF phase θ_j. Hence, the spinor components (α_n, β_n) characterise the overall rotation induced by the train of pulses. The spinors α and β are equivalent to the A and B polynomials with an additional linear phase

$$\begin{aligned} A_n &= z^{-n/2}\alpha_n \\ B_n &= z^{-n/2}\beta_n. \end{aligned} \tag{12}$$

Hence, A and B represent polynomials in z^{-1}. The symmetry results will be derived directly from the original recursion (Eq. (11)).

The derivation will follow the following steps: first we transpose both sides of Eq. (11), then we change the sign of the B_1 field and finally we equate the new matrix with Eq. (11). Transposing Eq. (11) leads to

$$\begin{bmatrix} \alpha_n & \beta_n \\ -\beta_n^* & \alpha_n^* \end{bmatrix} = \begin{bmatrix} C_1 & S_1 \\ -S_1^* & C_1 \end{bmatrix} \begin{bmatrix} z^{1/2} & 0 \\ 0 & z^{-1/2} \end{bmatrix} \cdot \begin{bmatrix} C_2 & S_2 \\ -S_2^* & C_2 \end{bmatrix} \cdots \begin{bmatrix} C_n & -S_n \\ -S_n^* & C_n \end{bmatrix}. \tag{13}$$

Changing the sign of the applied B_1 field alters the sign of each nutation angle ϕ_j, hence $\beta_n(\omega)$ experiences a sign change as well, while $\alpha_n(\omega)$ remains the same. This can be verified by inserting $n = 2$ in Eq. (11) and recurring it. Hence, the B_1 sign change leads to

$$\begin{bmatrix} \alpha_n & -\beta_n \\ \beta_n^* & \alpha_n^* \end{bmatrix} = \begin{bmatrix} C_1 & -S_1 \\ S_1^* & C_1 \end{bmatrix} \begin{bmatrix} z^{1/2} & 0 \\ 0 & z^{-1/2} \end{bmatrix} \cdot \begin{bmatrix} C_2 & -S_2 \\ S_2^* & C_2 \end{bmatrix} \cdots \begin{bmatrix} C_n & -S_n \\ S_n^* & C_n \end{bmatrix}, \tag{14}$$

which is a mirroring in time of the RF waveform plus a sign change in the RF phase θ. The $\beta_n(\omega)$ is complex conjugated in this equation as compared to Eq. (11), while $\alpha_n(\omega)$ remains unchanged.

Finally, we equate Eqs. (11) and (14). Refocusing pulses require linear-phase β, hence $\beta_n(\omega) = \beta_n^*(\omega)$. Examining the equality of Eqs. (11) and (14) on the right sides shows $S_n = S_1^*$ and more generally, by successively peeling off the sequence of matrices, $S_{n-j} = S_{j+1}^*$. Thus, the nutation angle (as governed by $|B_1|$) is symmetric while the phase θ is anti-symmetric. Note, that this is true for arbitrary choices of phase $\angle\alpha_n(\omega)$. However, changing the phase of α_n will change the B_1 waveform, while preserving the complex conjugate property of B_1.

References

[1] P.A. Bottomley, Spatial localization in NMR spectroscopy in vivo, Ann. N.Y. Acad. Sci. 508 (1987) 333–348.

[2] D.A. Yablonskiy, J.J. Neil, M.E. Raichle, J.J.H. Ackerman, Homonuclear J coupling effects in volume localized NMR spectroscopy: pitfalls and solutions, Magn. Reson. Med. 39 (2) (1998) 169–178.

[3] D.A.C. Kelley, L.L. Wald, J.M. Star-Lack, Lactate detection at 3T: compensating J coupling effects with BASING, J. Magn. Reson. Imaging 9 (5) (1999) 732–737.

[4] T. Lange, U. Dydak, T.P. Roberts, H.A. Rowley, M. Bjeljac, P. Boesiger, Pitfalls in lactate measurements at 3T, Am. J. Neuroradiol. 27 (4) (2006) 895–901.

[5] J. Frahm, K.D. Merboldt, W. Hänicke, Localized proton spectroscopy using stimulated echoes, J. Magn. Reson. 72 (1987) 502–508.

[6] J. Slotboom, A.F. Mehlkopf, W.M.M.J. Bovée, A single-shot localization pulse sequence suited for coils with inhomogeneous RF fields using adiabatic slice-selective RF pulses, J. Magn. Reson. 95 (1991) 396–404.

[7] M. Garwood, L. DelaBarre, The return of the frequency sweep: designing adiabatic pulses for contemporary NMR, J. Magn. Reson. 153 (2) (2001) 155–177.

[8] T.K.C. Tran, D.B. Vigneron, N. Sailasuta, J. Tropp, P. Le Roux, J. Kurhanewicz, S. Nelson, R. Hurd, Very selective suppression pulses for clinical MRSI studies of brain and prostate cancer, Magn. Reson. Med. 43 (1) (2000) 23–33.

[9] R.A. Edden, M. Schär, A.E. Hillis, P.B. Barker, Optimized detection of lactate at high fields using inner volume saturation, Magn. Reson. Med. 56 (4) (2006) 912–917.

[10] P. Le Roux, R.J. Gilles, G.C. McKinnon, P.G. Carlier, Optimized outer volume suppression for single-shot fast spin–echo cardiac imaging, J. Magn. Reson. Imaging 8 (5) (1998) 1022–1032.

[11] R.F. Schulte, J. Tsao, P. Boesiger, K.P. Pruessmann, Equi-ripple design of quadratic-phase RF pulses, J. Magn. Reson. 166 (1) (2004) 111–122.

[12] P. Le Roux, Procédé d'excitation radiofréquence dans une expérimentation de RMN, French Patent, FR8610179, 1986.

[13] J.B. Murdoch, A.H. Lent, M.R. Kritzer, Computer-optimized narrowband pulses for multislice imaging, J. Magn. Reson. 74 (1987) 226–263.

[14] G.B. Matson, M. Elliot, MATPULSE: an integrated program for selective RF pulse generation and pulse re-mapping with modulated gradients, Proc. Intl. Soc. Mag. Reson. Med. 3 (1995) 554.

[15] J.B. Murdoch, "Shinnar–Le Ruminations: reflections on pulse design and applications to in vivo spectroscopy, Proc. Intl. Soc. Mag. Reson. Med. 3 (1995) 552.

[16] J.M. Pauly, P. Le Roux, D.G. Nishimura, A. Macovski, Parameter relations for the Shinnar–Le Roux selective excitation pulse design algorithm, IEEE T. Med. Imaging 10 (1) (1991) 53–65.

[17] R.F. Schulte, A. Henning, J. Tsao, P. Boesiger, K.P. Pruessmann, Design of broadband RF pulses with polynomial-phase response, J. Magn. Reson. 186 (2007) 167–175.

[18] M. Shinnar, Reduced power selective excitation radio frequency pulses, Magn. Reson. Med. 32 (5) (1994) 658–660.

[19] S. Pickup, X. Ding, Pulses with fixed magnitude and variable phase response profiles, Magn. Reson. Med. 33 (5) (1995) 648–655.
[20] S. Pickup, M. Popescu, Efficient design of pulses with trapezoidal magnitude and linear phase response profiles, Magn. Reson. Med. 38 (1) (1997) 137–145.
[21] T.L. Hwang, A.J. Shaka, Water suppression that works. Excitation sculpting using arbitrary waveforms and pulse field gradients, J. Magn. Reson. A 112 (1995) 275–279.
[22] T.P.L. Roberts, T.A. Carpenter, L.D. Hall, A simple method for the construction of 180° refocusing RF pulses for use in nuclear magnetic resonance imaging, J. Magn. Reson. B 101 (1) (1993) 78–82.
[23] T.W. Parks, J.H. McClellan, Chebyshev approximation for nonrecursive digital filters with linear phase, IEEE Trans. Circuit Theory CT 19 (2) (1972) 189–194.
[24] A. Papoulis, Signal Analysis, McGraw-Hill, New York, 1977, ISBN 0070484600, Chapter 8.
[25] P. Le Roux, Suites régulières d'impulsions radio-fréquence en résonance magnétique. Applications à l'IRM, Ph.D. thesis, Universite Paris-Sud XI, 2006.
[26] P. Le Roux, R.F. Schulte, Predicting the energy of finite time RF pulses, Proc. Intl. Soc. Mag. Reson. Med. 15 (2007) 1673.
[27] D.E. Goldberg, Genetic Algorithms in Search, Optimization and Machine Learning, Addison-Wesley, Reading, MA, 1989, ISBN 0201157675.